

Kim, H.W. and Kenyon, A.R. and Duraisamy, K. and Brown, R.E. (2008) Interactional aerodynamics and acoustics of a propeller-augmented compound coaxial helicopter. In: 9th American Helicopter Society Aeromechanics Specialists' Meeting, 23-25 January 2008, San Francisco, California.

<http://strathprints.strath.ac.uk/27496/>

Strathprints is designed to allow users to access the research output of the University of Strathclyde. Copyright © and Moral Rights for the papers on this site are retained by the individual authors and/or other copyright owners. You may not engage in further distribution of the material for any profitmaking activities or any commercial gain. You may freely distribute both the url (<http://strathprints.strath.ac.uk>) and the content of this paper for research or study, educational, or not-for-profit purposes without prior permission or charge. You may freely distribute the url (<http://strathprints.strath.ac.uk>) of the Strathprints website.

Any correspondence concerning this service should be sent to The Strathprints Administrator: [eprints@cis.strath.ac.uk](mailto:eprints@cis.strath.ac.uk)

# Interactional Aerodynamics and Acoustics of a Propeller-Augmented Compound Coaxial Helicopter

<p>Hyo Won Kim*     Adam R Kenyon*</p> <p><i>Postgraduate Research Students</i></p> <p><i>Department of Aeronautics</i> <i>Imperial College London</i> <i>London SW7 2AZ</i> <i>United Kingdom</i></p>	<p>Karthikeyan Duraisamy</p> <p><i>Lecturer</i></p> <p><i>Department of Aerospace Engineering</i> <i>University of Glasgow</i> <i>Glasgow G12 8QQ</i> <i>United Kingdom</i></p>	<p>Richard E Brown</p> <p><i>Mechan Chair of Engineering</i></p>
--	---	--

## Abstract

The aerodynamic and acoustic characteristics of a generic hingeless coaxial helicopter with a tail-mounted propulsor and stabiliser have been simulated using Brown's Vorticity Transport Model. This has been done to investigate the ability of models of this type to capture the aerodynamic interactions that are generated between the various components of realistic, complex helicopter configurations. Simulations reveal the aerodynamic environment of the coaxial main rotor of the configuration to be dominated by internal interactions that lead to high vibration and noise. The wake of the main rotor is predicted to interact strongly with the tailplane, particularly at low forward speed, to produce a strong nose-up pitching moment that must be countered by significant longitudinal cyclic input to the main rotor. The wake from the main rotor is ingested directly into the tail propulsor over a broad range of forward speeds, where it produces significant vibratory excitation of the system as well as broadband noise. The numerical calculations also suggest the possibility that poor scheduling of the partition of the propulsive force between the main rotor and propulsor as a function of forward speed may yield a situation where the propulsor produces little thrust but high vibration as a result of this interaction. Although many of the predicted effects might be ameliorated or eliminated entirely by more careful or considered design, the model captures many of the aerodynamic interactions, and the resultant effects on the loading on the system, that might be expected to characterise the dynamics of such a vehicle. It is suggested that the use of such numerical techniques might eventually allow the various aeromechanical problems that often beset new designs to be circumvented — hopefully well before they manifest on the prototype or production aircraft.

## Notation

<p><math>A</math>     matrix of influence coefficients</p> <p><math>C_B</math>     blade loading coefficient</p> <p><math>C_D</math>     fuselage drag coefficient</p> <p><math>C_F</math>     rotor force coefficient</p> <p><math>C_M</math>     rotor moment coefficient</p> <p><math>C_P</math>     rotor power coefficient</p> <p><math>C_T</math>     rotor thrust coefficient</p> <p><math>C_W</math>     helicopter weight coefficient</p> <p><math>F</math>     vector of overall forces and moments</p> <p><math>K</math>     trim coupling matrix</p> <p><math>l</math>     fuselage half-length</p> <p><math>N</math>     number of fuselage panels</p> <p><math>N_b</math>     number of blades</p> <p><math>R</math>     rotor radius</p>	<p><math>U_\infty</math>     freestream velocity</p> <p><math>u</math>     local velocity</p> <p><math>w</math>     wake-induced velocity</p> <p><math>\alpha_s</math>     rotor shaft tilt</p> <p><math>\Gamma</math>     matrix of vortex loop strengths</p> <p><math>\theta</math>     array of control inputs</p> <p><math>\theta_0</math>     collective pitch angle</p> <p><math>\theta_{1s}</math>     sine cyclic pitch angle</p> <p><math>\theta_{1c}</math>     cosine cyclic pitch angle</p> <p><math>\mu</math>     advance ratio</p> <p><math>\psi</math>     blade azimuth</p> <p><math>\Omega</math>     rotor rotational speed</p> <p><b>subscripts/superscripts:</b></p> <p><math>c</math>     coaxial system</p> <p><math>l</math>     lower rotor of coaxial system</p> <p><math>u</math>     upper rotor of coaxial system</p> <p><math>t</math>     propulsor</p> <p><math>x, y, z</math>     orthogonal Cartesian components</p> <p><math>*</math>     trim target</p>
---	--

---

\* Currently at the Department of Aerospace Engineering, University of Glasgow as Visiting Researchers.

Presented at the American Helicopter Society Specialists' Conference on Aeromechanics, San Francisco, CA, 23–25 January 2008. Copyright © 2006 by the American Helicopter Society International, Inc. All rights reserved.

## Introduction

Helicopters that use a twin counter-rotating coaxial main rotor system have been under intermittent development since the early days of rotary-winged flight and several such machines have seen long and successful service (Ref. 1). Recent design studies have re-visited the coaxial configuration as one potential solution to future requirements for an efficient heavy-lift machine that is also capable of much higher forward flight speeds than conventional rotary-winged vehicles have traditionally been able to achieve.

Most helicopters rely on forward tilt of the rotor to produce the force required to propel the system through the air. With a conventional rotor system with low flapwise stiffness, the maximum performance of the system is often limited by the very high lift coefficients that are required at high advance ratio on the retreating side of the rotor disc in order to overcome the natural tendency of the rotor to flap backwards instead. The same is broadly true of a conventionally-articulated coaxial rotor. The situation alters dramatically though if significant flapwise stiffness is introduced into the system. The altered phase relationship between blade flapping and the applied aerodynamic load means that the rotor's natural tendency in forward flight is no longer to flap backwards but instead to produce a rolling moment about the rotor hub. In a coaxial system, the contributions to the rolling moment from the two contra-rotating rotors can be made to cancel, allowing the retreating sides of the rotors to be flown at a much lower average lift coefficient than with a conventional rotor. The premise is that such rotors can thus be flown to much higher advance ratios than conventional single main rotor designs before the aerodynamics of the retreating blades pose a serious limit to the performance of the system. This is the basis of the Advancing Blade Concept (ABC) rotor developed by Sikorsky in the 1970s. The history of the development of this system as part of the XH-59A prototype helicopter is documented comprehensively by Burgess in Ref. 2.

The equivalent argument in terms of speed rather than advance ratio is weakened somewhat by the fact that compressibility on the advancing side of the rotor at high forward speed poses as great an impediment to the performance of a stiffened coaxial rotor as it does to a conventional system. This is particularly so if the rotors are highly loaded, for instance through being required to produce a significant proportion of the propulsive force required by the aircraft. Wings or an auxiliary propulsion system can be added to the aircraft, to yield a lift- or thrust-compounded configuration (possibly, as on the XH-59A, in conjunction with a variable-speed rotor), reducing the load on the main rotor

and thus ameliorating the effects of compressibility on the performance of the vehicle at high forward speed. For this reason, the thrust compounded, stiffened coaxial rotor is considered to be a very strong contender to form the basis of a new generation of heavy-lift, high-speed rotorcraft. The XH-59A itself used a pair of turbojets to augment the thrust produced by the main rotor, but despite the considerable effort that was put into testing scaled models and prototype aircraft, this design did not reach production. The concept has been revived more recently though in the development of Sikorsky's X2 technology demonstrator. This helicopter is likely to adopt a tail-mounted pusher propeller to augment the propulsive force that is provided by its ABC-type coaxial rotor.

This particular configuration, although showing significant promise as a viable technological solution to operational requirements for increased helicopter forward speed, manoeuvrability and load-carrying ability, is inherently very complex from an aerodynamic point of view. Under certain flight conditions, the performance and flight mechanics of such a configuration are likely to be influenced very strongly by aerodynamic interactions between the various components of the helicopter. In order to maximise the efficiency and potential of this type of aircraft, a thorough understanding of the nature and form of the aerodynamic interactions that occur within the system, as well as an appreciation of the flight conditions under which such interactions might pose the greatest challenges to the operation and control of the vehicle, is essential (Ref. 3).

The system that is analysed in this paper has a stiff coaxial rotor system, mounted above a compact but streamlined fuselage, together with a rear-mounted pusher propeller to augment the thrust of the main rotor. Instead of focusing on the properties of any specific, real vehicle, the configuration that is analysed in this paper is entirely fictitious. Various pertinent characteristics of the thrust-compounded coaxial configuration have been synthesised to obtain a generic representation of this class of helicopters, in the hope that predictions of the aerodynamic environment of the generic configuration might shed some light on the behaviour of this class of helicopters as a whole. Nevertheless, many of the properties of the various components of the generic system have been simplified considerably from those of any real design, and it should be borne in mind that it is highly likely that most of the various aerodynamic pathologies that appear to be attributed to this configuration by this study could be ameliorated fairly easily through sensible engineering design or simple geometric modification.

For many years, the aim of the developers of computational tools for the analysis of rotorcraft

has been to develop a method that can be used very early in the design process to inform the designers of such aircraft of the potential aerodynamic problems that might arise from injudicious juxtaposition of the various elements of their proposed configuration. The ideal has always been for this information to become available to the designers well before any such problems might manifest on the prototype or production vehicle (Ref. 4). Unfortunately, the historical record shows past efforts in this regard to have met with limited success (Refs. 5–10).

The aim of this paper is thus to demonstrate some progress in the computational modelling of helicopter interactional aerodynamics, and to suggest perhaps that the state of the art of computational helicopter aerodynamic predictions is advancing to a stage where some insight into the detailed features of aerodynamic interactions in a system as aerodynamically complex as a propeller-augmented hingeless coaxial helicopter can be obtained. To this end, computational predictions of the aerodynamics and acoustics of the generic thrust-compounded coaxial helicopter are compared and contrasted at various forward flight speeds.

## Computational Model

The aerodynamic behaviour of a generic, thrust-compounded coaxial helicopter has been simulated using the Vorticity Transport Model (VTM), developed by Brown (Ref. 11) and extended by Brown and Line (Ref. 12). A full description of the model is contained within the original references; for the sake of brevity only the basic characteristics of the model are summarised here.

The VTM solves the vorticity-velocity form of the Navier-Stokes equations on a Cartesian grid surrounding the rotorcraft. Significant savings in memory and computational time are achieved by allowing the distribution of cells within the computational domain to track the vorticity field as it evolves. This is done by creating computational cells in regions of the flow where vorticity exists and subsequently destroying them once the vorticity migrates elsewhere. Computational efficiency is enhanced further by using a sequence of nested grids in which the cells within the outer grids are arranged to be coarser than those closer to the rotor. This reduces the overall cell count whilst allowing a highly resolved flow field to be maintained near the rotor. The convection algorithm implemented in the VTM is particularly effective in controlling the local rate of dissipation of the vorticity, allowing the integrity of vortical structures in the rotor wake to be preserved for many rotor revolutions. The VTM is thus particularly

well suited to resolving the wake-induced interactions between geometrically well-separated components of the aircraft. In the context of the present paper, this property of the model enables the long-range aerodynamic interactions between the twin main rotors, the tail propulsor and the horizontal stabiliser of the propeller-augmented coaxial helicopter to be studied in detail.

In the version of the VTM used to generate the results presented in this paper, the blade aerodynamics are modelled using an extension of the Weissinger-L version of lifting line theory. In this approach, the two-dimensional aerodynamic characteristics of the rotor blade sections are specified in a look-up table as a function of angle of attack and Mach number for a given Reynolds number. These characteristics are then enforced by applying a modified zero through-flow condition on a set of aerodynamic stations along the length of each blade. Even though blade stall can be modelled using this technique, the approach is still essentially inviscid. The profile drag of the blade is thus calculated as a separate function of local angle of attack and then added to the local aerodynamic force that is calculated from the lifting line model.

To model the presence of a fuselage, the fuselage surface is discretised into a system of  $N$  quadrilateral panels. Each panel edge is represented as a vortex filament of constant strength  $\Gamma_i$ , with the filaments on each panel  $i$  thus forming a closed loop of vorticity. The velocity at any panel centroid is then given by the sum of the influences from all vortex filaments on the body together with the velocity  $w$  that is induced by any other vorticity within the flow and the freestream component of velocity,  $U_\infty$ . A boundary condition of zero through-flow is enforced simultaneously at the centroids of all panels, so that

$$(U_\infty + w)_i \cdot \mathbf{n}_i + \sum_{j=1}^N A_{ij} \Gamma_j = 0 \quad (1)$$

where  $\mathbf{n}_i$  is the unit vector normal to panel  $i$ . This linear equation is solved at each computational timestep to obtain the matrix of vortex loop strengths,  $\Gamma$ . The influence matrix,  $A$ , accounts for the velocity induced on each panel by every other panel, and is thus of size  $N$  by  $N$ . The fact that the fuselage is closed provides an additional, but implicit, constraint on the relationship between the panel strengths, by requiring that they should sum to zero, that results in  $A$  being singular. In the VTM, the vortex loop strengths are thus evaluated using an approximation to the inverse of  $A$  that is obtained using Singular Value Decomposition. A considerable saving in computational effort is achieved by assuming the fuselage to be rigid. This is because the matrix of influence coefficients

does not then change with time, allowing the inversion of  $A$  to be performed prior to the simulation.

The pressure on the fuselage surface is calculated from the unsteady Bernoulli equation,

$$\frac{p - p_\infty}{\frac{1}{2}\rho} = U_\infty^2 - |\mathbf{u}|^2 - 2\frac{\partial\phi}{\partial t} \quad (2)$$

In the VTM, the change in panel strengths with time as well as the disturbance to the velocity potential due to the convection of vortices within the wake are accounted for when evaluating the unsteady potential term  $\partial\phi/\partial t$ . Similarly, the contribution from all the vorticity in the computational domain, as well as a near-field correction term that accounts for the self-influence of the vorticity on each panel by assuming it to be distributed as an equivalent vortex sheet, is accounted for when evaluating the velocity  $\mathbf{u}$  on the surface of the fuselage.

Lift generation by the fuselage is modelled in the VTM by applying the Kutta condition along pre-specified separation lines on the surface of the fuselage. The Kutta condition is satisfied by ensuring that the net circulation around the separation line is zero, and this is enforced in the VTM by releasing into the wake an amount of vorticity that is equal in strength to the difference between the strengths of the panels on either side of the separation line. The vorticity that is created as a consequence of the generation of lift is sourced into the VTM grid, where it feeds back into the loading produced on the system. The circulatory contribution to the unsteady aerodynamic characteristics of any lifting surface in the flow is thus fully represented. Note though that the viscous wake of the non-lifting components of the configuration is not accounted for at present.

Elements of this model have been used before to investigate the aerodynamic interactions experienced by a generic helicopter configuration (Ref. 13), and the procedure described above has been shown to produce very good agreement with experimental results for the mean and time-dependent variation of inflow through the rotor, the position of the vortices within the rotor wake as they approach the surface of the fuselage, and both the mean and time-variation of the pressure fields that are induced on the surface of the fuselage by these vortical structures. The model has also been used to investigate the aerodynamic behaviour of isolated coaxial rotors (Ref. 14) and has been shown to capture accurately the performance of such systems. These previous studies provide some confidence that the model is able to capture those features of the aerodynamic environment of the vehicle that are of most relevance to the present study.

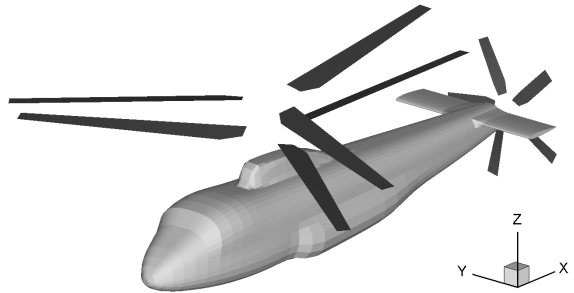


Figure 1: *Generic thrust-compounded hingeless coaxial configuration.*

## Description of Simulated Configuration

This paper analyses the aerodynamic interaction between the components of a generic helicopter configuration that comprises a stiffened twin coaxial rotor system together with an auxiliary tail propeller, or ‘propulsor,’ to augment the propulsive thrust that is produced by the main rotor system (see Figure 1). Each of the components of this configuration is described in detail below. Although the inspiration for much of the geometry of the configuration is derived from helicopters such as the XH-59A and X2, it should be borne in mind throughout that significant simplifications have been introduced in many instances in order to allow the results presented in this paper to represent more straightforwardly the generic characteristics of such a configuration rather than the specifics of any one particular aircraft.

### Rotor System

The main rotor system modelled in this study follows closely that of the XH-59A’s ABC rotor in terms of its geometry. Two counter-rotating, three-bladed rotors are separated axially by a distance of  $0.139R$ . The blades of both rotors are tapered linearly in planform and have  $-10^\circ$  of non-linear twist. For simplicity, however, a constant airfoil section, NACA 23012, is used along the entire span of the rotor blades. While the use of constant blade sections yields a rather crude representation of the sophisticated design of real ABC-type rotor blades, the resulting wake structure, and hence the aerodynamic interference between the main rotor system and the other lifting devices in the configuration, should nevertheless be sufficiently representative of a realistic full-scale vehicle of this type. The geometric properties of the main rotor system are summarised in Table 1.

In all simulations presented in this paper, the flapwise stiffness of ABC-type rotors is approximated by assuming the rotor blades and their

Table 1: *Main rotor and propulsor geometries*

	Main Rotor	Propulsor
Rotor radius	$R$ (5.5m)	$R_t$ (0.28 $R$ )
Number of rotors	2	1
Blades per rotor	3	5
Rotor separation	0.139 $R$	–
Root cutout	0.12 $R$	0.20 $R_t$
Solidity	0.127	0.222
Twist	$-10.0^\circ$	$-30.0^\circ$
Chord	Tapered (2:1)	0.18 $R_t$
Airfoil sections	NACA 23012	NACA 0012

attachments to the rotor hub to be completely rigid. Although this simplification may appear to be rather crude, and of course the flap-lag dynamics of the blades is suppressed entirely using this approach, the loading on the rotors and the resultant wake geometry of such a system has been shown to be very similar (Ref. 15) to that of rotors with the high level of flapwise stiffness that is characteristic of the coaxial rotors of ABC-type systems (Refs. 16, 17). Thus, as far as the effects of aerodynamic interference are concerned, the simplified rigid rotor model is expected to provide a very close representation of the aerodynamic environment that is generated by practical semi-rigid coaxial rotor systems.

The twin rotors of the coaxial system are arranged so that the upper rotor rotates anticlockwise and the lower rotor rotates clockwise when viewed from above. The rotors have been arranged to overlap when blades from both the upper and the lower rotors pass directly over the centreline of the rear fuselage. For simplicity, the hub of the rotor is not modelled in the simulations, but it should be realised that the omission of this feature of the system will have some effect on the physical plausibility of the predicted structure of the wake immediately downstream of the rotor shaft.

## Auxiliary Propulsor

A five-bladed propeller is used to represent an auxiliary thrust-producing device mounted in pusher configuration to the rear of the fuselage. The blades of this propulsor feature a tapered root end,  $-30^\circ$  of linear twist, and a NACA 0012 sectional profile. The propulsor is mounted so that its rotational axis is aligned with the longitudinal axis of the aircraft. Its rotational speed is fixed at 4.25 times the main rotor speed and its direction of rotation is clockwise when seen from the rear of the aircraft.

The pitch angle of all the blades of the propulsor is adjusted simultaneously to produce the desired level of thrust in much the same manner as the collective pitch control affects the feathering of the blades of the main rotors. The blades of the

Table 2: *Fuselage geometry*

Fuselage length ( $2l$ )	2.04 $R$
Tailplane :	
Airfoil section	NACA 0012
Span	0.667 $l$
Chord	0.167 $l$
Hub x,y,z coordinates:	
Main rotor (lower)	0.765 $l$ , 0.000 $l$ , 0.386 $l$
Main rotor (upper)	0.765 $l$ , 0.000 $l$ , 0.522 $l$
Propulsor	2.079 $l$ , 0.000 $l$ , 0.111 $l$
(relative to fuselage nose)	

propulsor and their attachments to their hub are otherwise assumed to be rigid. Note that, as with the main rotor system, the hub of the rotor itself is not modelled. A summary of the geometry of the propulsor is given in Table 1.

## Fuselage Geometry

The modelled configuration includes a fuselage as shown in Fig. 1. The geometry of the fuselage is entirely fictitious but was selected to be representative of the compact but streamlined configuration of modern high-performance helicopters. The fuselage features a large horizontal tail surface to allow the effects of aerodynamic interactions that might arise as a consequence of the rotorcraft featuring a lifting empennage arrangement to appear in the simulations. Indeed, the aerodynamic interaction between the wake from the main rotor and the empennage has been documented as being responsible for a number of unexpected flight mechanic issues in modern helicopters (e.g. Refs. 8–10). The tail surface is untwisted and has a rectangular planform, and the Kutta condition is satisfied along its entire trailing edge. This allows it to act as a lifting surface and to produce a representative wake structure. Other relevant properties of the fuselage are summarised in Table 2.

## Trim Methodology

The trim algorithm implemented in the VTM drives the rotor controls so that their rates of change are proportional to the difference between the current values and the prescribed target values of the components of an array of forces and moments that represent the overall loads on the vehicle. Given the  $xyz$ -coordinate system shown in Fig. 2, the array

$$F = [ C_{Fx}, C_{Fy}, C_{Fz}, C_{Mx}, C_{My}, C_{Mz} ] \quad (3)$$

contains the Cartesian components of the overall forces and moments that are applied by the rotor system to some suitable reference point on the airframe. For present purposes the system is assumed

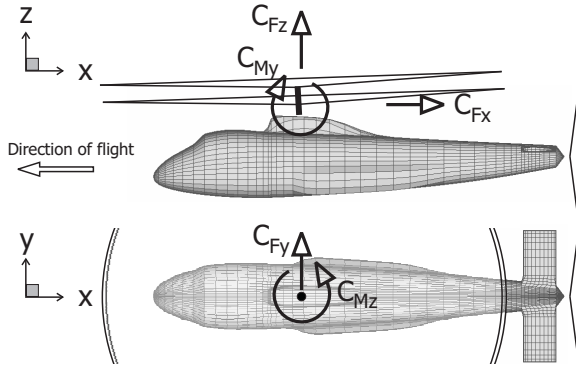


Figure 2: Schematic showing the axis convention for forces and moments.

to be in trim when there is zero net moment about the base of the main rotor mast and simultaneously the propulsive force matches the drag on the vehicle and the weight of the aircraft is balanced by the vertical component of the force produced by the rotors. This trim state is imposed on the system by defining the array

$$F^* = [-C_D, 0, C_W, 0, 0, 0] \quad (4)$$

of prescribed target loads on the vehicle. Given control inputs  $\theta^u = [\theta_0^u, \theta_{1s}^u, \theta_{1c}^u]$  and  $\theta^l = [\theta_0^l, \theta_{1s}^l, \theta_{1c}^l]$  to the upper and lower rotors respectively, and  $\theta^t = [\theta_0^t]$  to the propulsor, the trim algorithm used in the VTM can be written as

$$\begin{bmatrix} \dot{\theta}^u(t) \\ \dot{\theta}^l(t) \\ \dot{\theta}^t(t) \end{bmatrix} = K (F^* - F(t)) \quad (5)$$

where  $K$  is a  $7 \times 6$  coupling matrix that prescribes the rate at which each of the controls should respond to any discrepancy between  $F^*$  and  $F$ . This simple first-order dynamical system serves essentially as a simplistic pilot model that adjusts the controls continuously during a simulation to drive the loads on the system towards their prescribed values. The dynamic nature of this approach requires the system to be considered to be in trim only when  $\bar{F} = F^*$ , where  $\bar{F}$  is the long-term average of  $F(t)$ , but no further assumptions regarding the frequency content of the loading on the system are required to establish a steady-state operating condition. The approach is thus ideal for the analysis of flight cases where aerodynamic interactions between the various components of the system might not necessarily result in periodic long-term behaviour of the loads on the vehicle. A more detailed account of the trim model is contained in Ref. 15.

In all simulations presented in this paper, the collective pitch inputs to both upper and lower rotors are varied together to alter the total thrust produced by the system while differential collective pitch input to the upper and lower rotors is

Table 3: Simulated flight conditions and corresponding trim targets.

Speed	Weight	Drag	Shaft tilt
$\mu$	$C_W$	$C_D$	$\alpha_s$
0.05	0.012	0.00008	$0^\circ$
0.10	0.012	0.00032	$0^\circ$
0.15	0.012	0.00072	$4^\circ$
0.30	0.012	0.00288	$4^\circ$

used to maintain zero net yawing moment on the system. The XH-59A employed differential cyclic pitch input to optimise the performance of the rotor (Refs. 2, 17–19), but in the present analysis this complication is avoided and the same cyclic pitch inputs are applied simultaneously to both upper and lower rotors to generate the required rolling and pitching moments on the system.

The rigidity of the main rotor system limits the ability of the cyclic pitch controls to tilt the tip path plane relative to the rotor shaft in order to produce a propulsive thrust component to the system, but the high control power of the stiffened system allows very direct control of the pitch attitude of the aircraft and hence the shaft tilt with respect to the flightpath. The balance of propulsive force between the main rotor system and propulsor that is required to maintain a given forward flight speed is thus largely controlled by the pitch moment that is demanded from the main rotor system. Representation of this characteristic of the helicopter needs to be approached with some care since the rigid-body dynamics of the fuselage is not modelled directly. The approach taken was to assume that, at very low forward speed, just sufficient pitching moment is demanded from the main rotor to maintain its shaft perpendicular to the flightpath, but, beyond an advance ratio of 0.10, additional pitching moment is demanded from the main rotor to force its shaft to incline  $4^\circ$  forward, thereby allowing the main rotor to contribute partially to the forward thrust that is required to maintain the forward speed of the helicopter. Any deficit in the propulsive force that is generated by the main rotor is then provided by the tail propulsor by suitable variation of its own collective pitch.

The required propulsive force is calculated by assuming the parasite drag of the system to be represented by an equivalent flat plate (Ref. 20) with  $1/25^{th}$  of the main rotor disc area. This yields a quadratic variation of the required propulsive force with forward speed that is comparable, in non-dimensional terms, to that of the XH-59A (Ref. 21). The weight of the aircraft was assumed to be balanced throughout by a vertical component to the thrust coefficient that is produced by the system of 0.012, this again being representative of an aircraft of the size of the XH-59A. The range

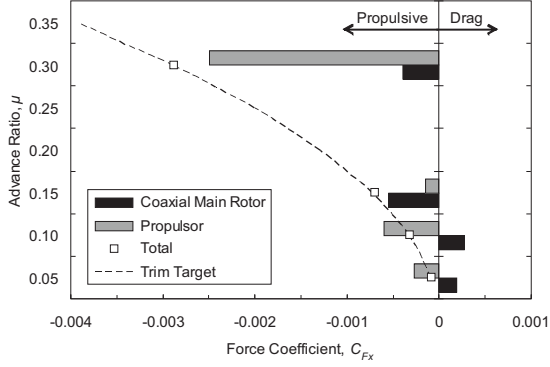


Figure 3: *Partition of the propulsive force between the main rotor and propulsor as a function of forward speed.*

of forward speeds for which calculations were performed, and the corresponding trim targets for the simulations are summarised in Table 3.

## Aircraft Performance

Figure 3 shows the variation with forward flight speed of the propulsive force that is required to overcome the drag of the aircraft given the model described above. At low forward speed, the absence of any forward tilt of the main rotor causes it to generate an in-plane component of force that has to be counteracted by the propulsor in order to produce the requisite propulsive force on the configuration. This is certainly non-optimal and results in a higher consumption of power at low forward speed than is necessary, as is shown in Fig. 4 where the overall power consumption of the system is plotted as a function of advance ratio. It is likely though that this flaw could be corrected through a more refined scheduling of the shaft tilt with forward speed than that adopted here. Indeed, the forward tilt of the rotor shaft that is scheduled at advance ratios greater than 0.10 allows the main rotor to contribute to the propulsive force that is required to overcome the drag of the system, and translates into a marked reduction in the power that is consumed by the main rotor at higher forward speed, as shown in Fig. 4. This observation needs to be placed in context, though. By partitioning the power consumption into the individual contributions from the main rotor and propulsor, Fig. 4 also reveals that, although the power consumed by the main rotor can be reduced quite considerably by unloading the system in favour of the propulsor, this advantage can be outweighed by the power requirements of the propulsor itself at high forward flight speeds.

Finally, Fig. 5 shows the partition of the pitching moment into the individual contributions that are generated by the main rotor system, the propulsor

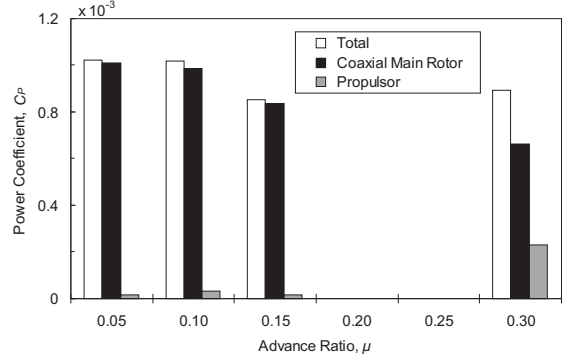


Figure 4: *Partition between the main rotor and propulsor of the power required by the vehicle as a function of forward speed.*

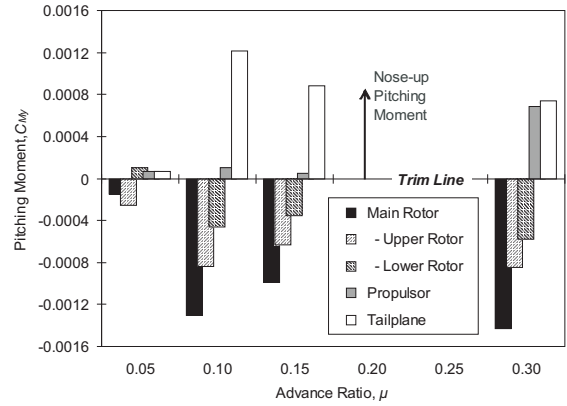


Figure 5: *Partition between the main rotor, propulsor and tailplane of the pitching moment required to trim the vehicle as a function of forward speed.*

and the horizontal tailplane in order to maintain the aircraft in trim at the various forward speeds that were simulated. The origin of the very large contribution to the overall pitching moment from the tailplane, particularly at low forward speeds, will be discussed later in this paper. The contribution of the tailplane translates into a significant variation with forward speed in the pitching moment that must be commanded by cyclic input into the main rotor system in order to maintain overall zero pitching moment on the configuration and hence the aircraft in trim. The requirement on the main rotor to produce this moment will be shown shortly to result in a significant elevation in the loading on the rear of both the upper and lower rotors of the coaxial system, particularly at low forward speed, that has interesting consequences particularly for the vibration and the acoustic radiation that is produced by the configuration.

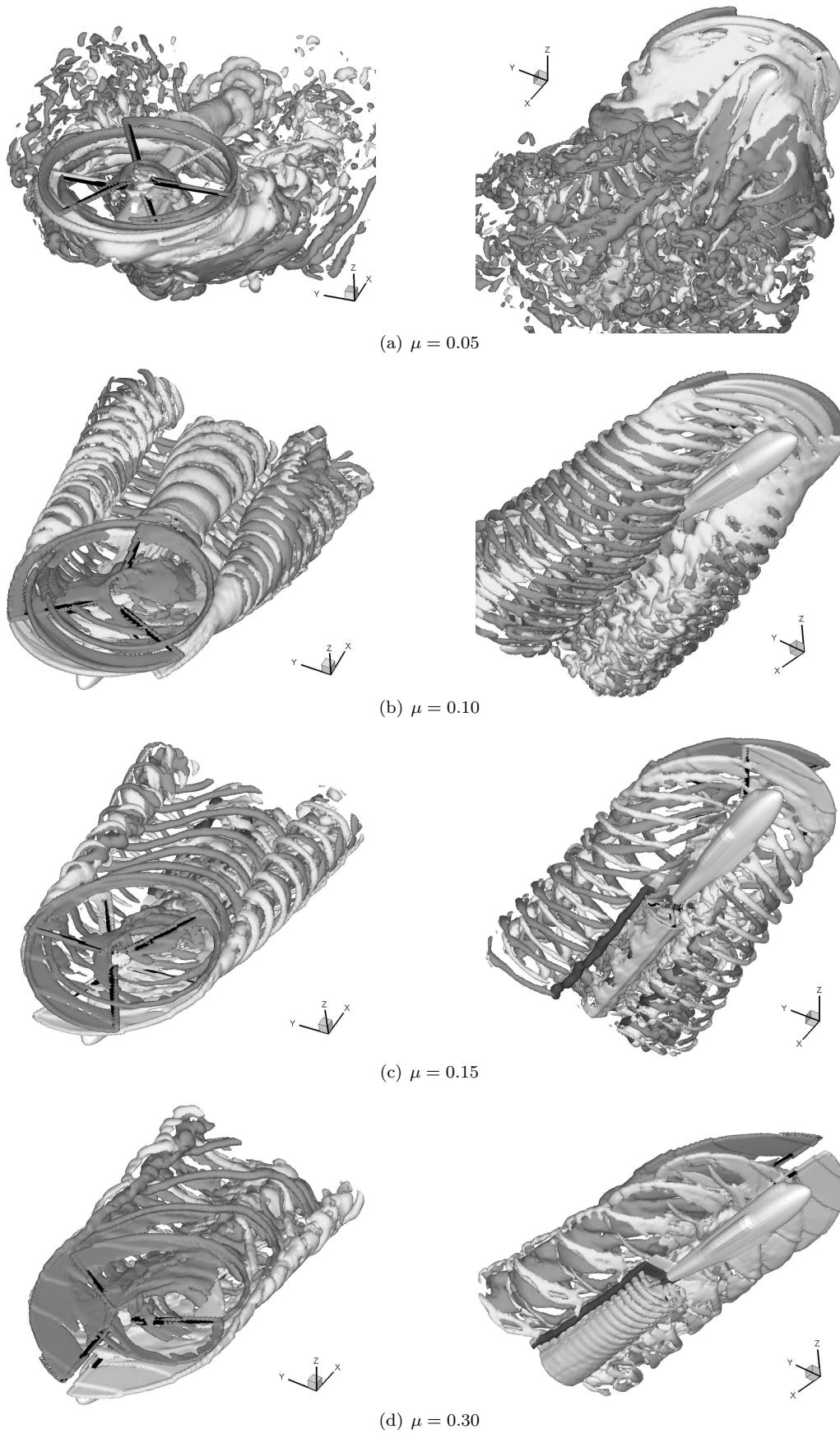


Figure 6: *Visualisation of the wake structure of the full configuration in steady forward flight at various advance ratios. Wakes from the different elements of the configuration coloured in separate shades of grey. (Left: top view. Right: bottom view.)*

## Wake Structure

Figure 6 shows a series of snapshots of the structure of the wake that is generated by the helicopter at each of the advance ratios that was simulated. In each plot, a set of iso-surfaces is presented on which the vorticity in the flow around the vehicle has constant magnitude. The wakes that are generated by each of the main rotors, the tail propulsor and the horizontal tail surface are coloured separately in various shades of grey. To aid in the interpretation of these figures, Fig. 7 reveals the relative extent of the wake envelope that is associated with each rotor by plotting the trajectories of their tip vortices as they intersect the plane of lateral symmetry of the fuselage.

Figures 6(a) and 7(a) show the wake of the helicopter when operating at an advance ratio  $\mu = 0.05$ . At this forward speed, the wake of the main rotor system is in a transitional state between the cylindrical, hover-like form that it would adopt at lower advance ratios and the flattened, aeroplane-like form that is characteristic of the system at higher advance ratios. The precursors of the rolled up super-vortices that form at the sides of the wake at higher advance ratios are clearly evident, but at this forward speed these structures are highly unsteady and their formation is continually disrupted by the destabilising effect of the mutual interaction between the individual tip vortices that constitute the underlying helicoidal structure of the wakes of the rotors. This results in significant disorder in the wake a fairly short distance downstream of the tail as the products of this instability interact to form progressively smaller coherent structures. The view from below shows the very strong influence of the fuselage in displacing the wake of the main rotors, to the extent that a powerful bow-shaped vortex forms as a result of the retardation and confluence of several tip vortices near a stagnation point on the upper surface of the forward fuselage. The arms of this vortex trail down the sides of the fuselage and interact with the developing super-vortices on both sides of the aircraft. Figure 8 shows the wake from the rear of the main rotors to impinge on the fuselage just slightly forward of the tailplane. The marked downwards trajectory of the wake from the main rotor results in very little direct interaction between the main rotor and the propulsor; although some vorticity is indeed ingested into the bottom of the propulsor disc, and some also rolls backwards along the top surface of the fuselage to interact with the tailplane, most of the vorticity created by the main rotors can be seen to pass below the propulsor at this forward speed. The very obvious skewing of the wake seen in Figure 9 of the propulsor to the port side of the aircraft suggests a powerful indirect interaction between the main

rotor system and the propulsor, although part of this effect might be due to the almost complete entrainment of the wake of the tailplane through the propulsor disc at this forward flight speed.

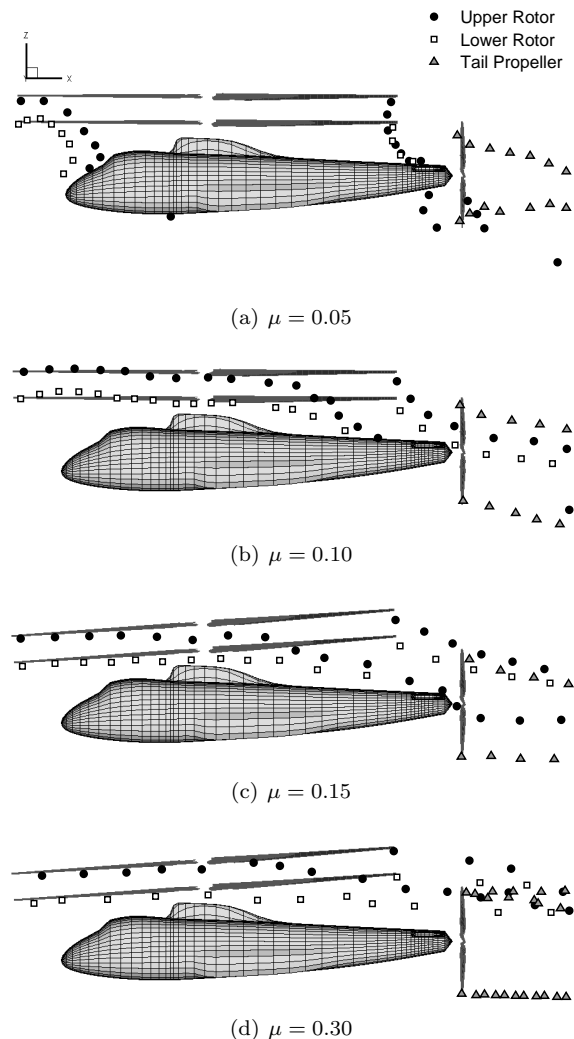


Figure 7: *Trajectories of the tip vortices of the main rotors and propulsor. (Each plot is a composite showing the points of intersection of individual vortices with the longitudinal plane through the fuselage centreline at various times during a single main rotor revolution.)*

Figures 6(b) and 7(b) show the wake of the helicopter when operating at a slightly higher advance ratio ( $\mu = 0.10$ ). At this forward speed, the individual tip vortices from the blades of the main rotors interleave and co-orbit to form a pair of highly-structured super-vortices along both sides of the wake. As at the lower flight speed, the wake from the tailplane is again entrained almost completely into the propulsor; the presence of the two powerful, counter-rotating vortices from the tips of the tailplane at this forward flight speed results in significant flattening of the wake tube of the propulsor a short distance downstream of the aircraft. The indirect interaction between the propulsor and the

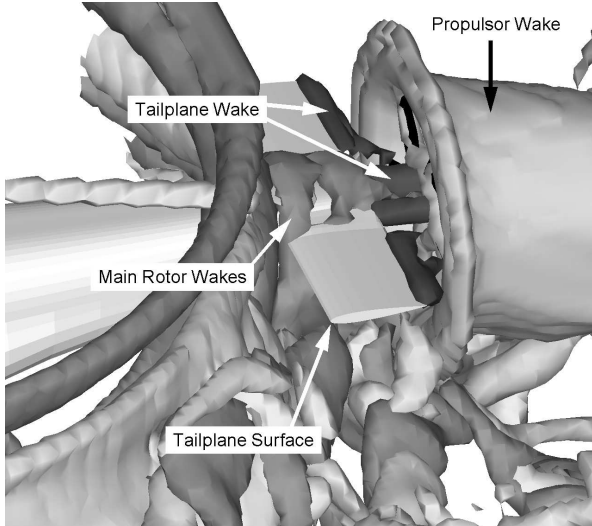


Figure 8: *Visualisation of the wake structure of the configuration, showing the distortion of the tip vortices around the fuselage and tailplane at advance ratio  $\mu = 0.05$ .*

main rotor results in a strong modulation of the vorticity in the wake tube of the propulsor to form a series of toroidal structures that have a characteristic wavelength that is very similar to the spacing between the individual tip vortices from the main rotor system. This modulation is most likely enhanced by the rather obvious and very direct impingement of tip vortices from the main rotor system on the tail of the configuration at this flight speed. Indeed, Fig. 10(a) shows a succession of tip vortices from the main rotor to pass very closely over the upper surface of the tailplane, subsequently to be ingested directly into the upper half of the propulsor (see Fig. 10(b)). The effect of this powerful interaction between the main rotor and the tail of the configuration on the loading on the helicopter is discussed in the next section of this paper.

Figures 6(c) and 7(c) show the wake of the system when flying through the air at advance ratio  $\mu = 0.15$ . At slower flight speeds the root vortex system that is generated by the main rotors is helicoidal in structure and is only moderately skewed. Interaction of this vortex system with the other components of the configuration is thus generally limited to a direct impingement on the fuselage, well forward of the tailplane (as shown in Figure 10), in such a way that the individual vortices encounter the fuselage at such a steep angle that they do not tend to propagate far along the length of the body before being swept away into the flow below the helicopter. At low forward flight speed the root vortex system thus does not tend to interact with the tailplane. Figure 11(a) shows the root vortex system that is generated by the main

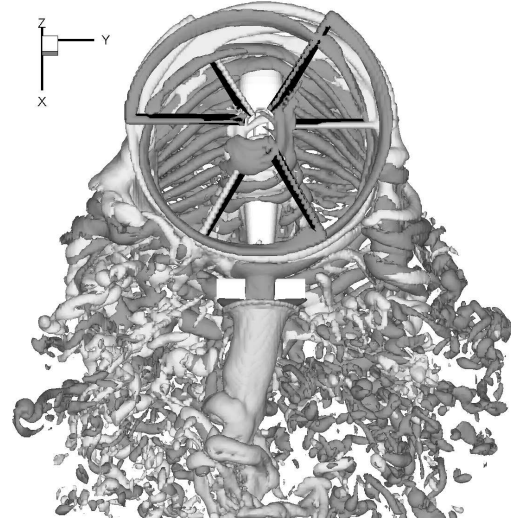
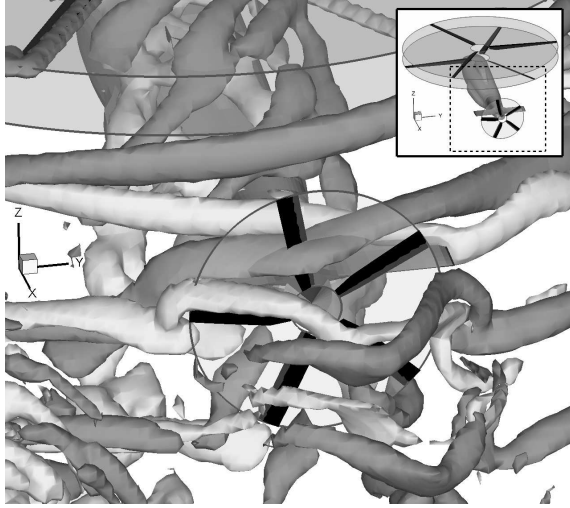


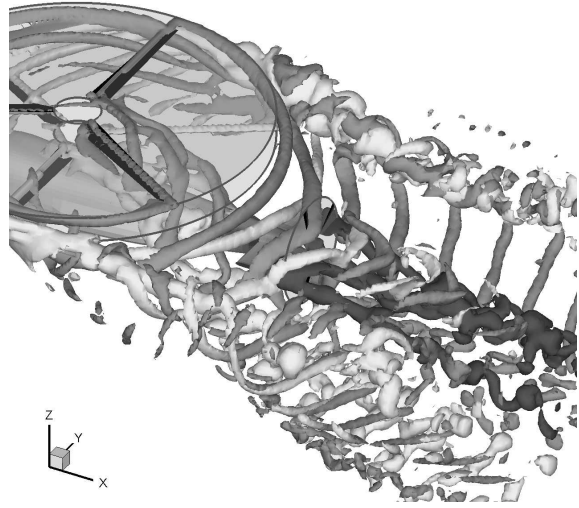
Figure 9: *Visualisation of the wake structure of the configuration: view from above at advance ratio  $\mu = 0.05$  showing the incipient formation of super-vortices in the wake of the main rotor and the interaction-induced skewing of the propulsor wake.*

rotors at higher advance ratio to roll up into a pair of concentrated structures that trail down the sides of the fuselage. At  $\mu = 0.15$  these structures are biased strongly towards the port side of the fuselage. As shown in Fig. 11(b), the port-side vortex interacts very strongly with the tailplane, producing a corkscrew-like perturbation to the trailing vortex that is produced by the port side of this surface. Further downstream, the root vortex structure causes significant disruption to the structure of the wake tube of the propulsor, forcing it to roll up along its port edge and to skew to such an extent that the trailing vortex from the starboard tip of the tailplane is no longer entrained into the wake of the propulsor but instead is able to convect without significant interference into the flow downstream of the helicopter (see Fig. 6(c)).

As the advance ratio of the system is increased, the effect of the main rotor wake in modulating the structure of the wake produced by the propulsor steadily decreases, to the extent that at the highest advance ratio that was simulated ( $\mu = 0.30$ ) this effect is almost entirely absent, as can be inferred from the very orderly, helical structure of the wake produced by the propulsor that is shown in Fig. 6(d). Similarly, the amount of vorticity from the main rotor system that is entrained directly through the propulsor disc decreases significantly as the rearwards skew of the wake of the main rotor increases with forward speed of the aircraft. This can be seen by comparing Fig. 11(a), which shows a significant proportion of the vorticity that is produced from the tips of the main rotor to be entrained into the upper half of the propulsor at

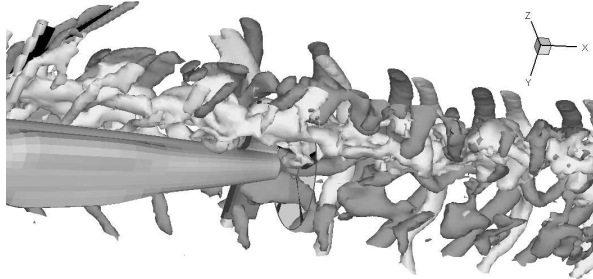


(a) Close-passage and impingement of the tip vortices from the main rotors on the upper surface of the tailplane. (Tailplane wake not visualised for clarity.)

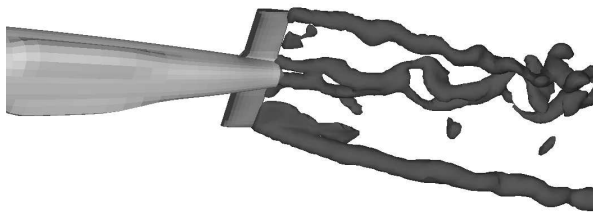


(b) Ingestion of the main rotor vortices through the propulsor showing subsequent distortion due to interaction with propulsor and tailplane wake.

Figure 10: Visualisation of the wake structure of the configuration, showing the distortion of the flow around the tail at advance ratio  $\mu = 0.10$ . (Propulsor wake not visualised for clarity.)



(a) View showing the formation of a concentrated root vortex structure from the main rotor and its subsequent impingement on the tailplane.



(b) View showing the distortion of the tailplane wake under the influence of the main rotor root vortices and the propulsor.

Figure 11: Visualisation of the wake structure of the configuration, showing the distortion of the flow around the tail at advance ratio  $\mu = 0.15$ . View from below the port side of the aircraft. (Propulsor wake not visualised for clarity.)

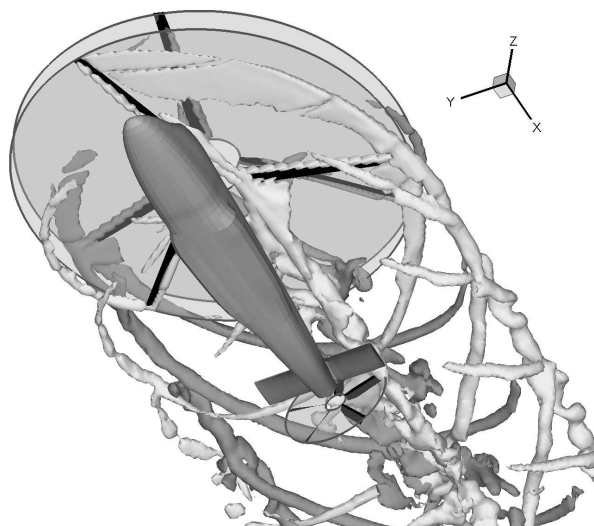
an advance ratio of 0.15 (see also Fig. 7(c)), with Fig. 12 which shows minimal such entrainment at an advance ratio of 0.30 (see also Fig. 7(d)).

## Interactional Aerodynamics

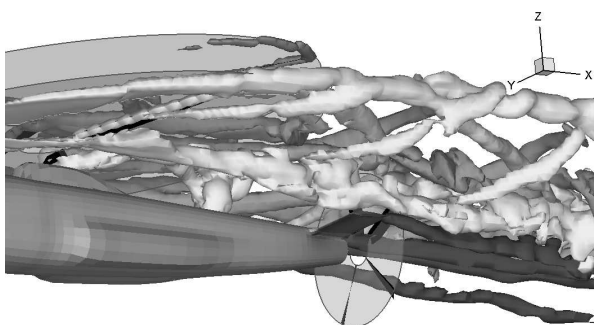
It is thus possible to conceive of two rather different modes of aerodynamic interaction taking place within the system (Ref. 22). The first, rather obvious ‘direct’ mode involves the direct impingement of the wake of one of the components of the system on the other, and thus a direct and strong modification of the aerodynamic environment experienced by the affected component and hence its loading. The second ‘indirect’ mode, where interaction between the wakes of the two components — perhaps even at quite some distance from the components themselves — modifies the geometry of both wakes, and thus feeds back into the aerodynamic environment of the system and hence its loading in a far more subtle way than in the first case, is clearly evident in some of the images presented in Fig. 6. This section of the paper examines in more detail the effects of these aerodynamic interactions on the loads produced within the system.

## Rotor-Rotor Interaction

Figure 13 shows the distribution of inflow that is experienced by the upper and lower rotors of the coaxial system at each advance ratio that was simulated. Each individual plot shows the radial distribution of inflow that is experienced by a single blade, during a single rotor revolution, as a polar



(a) View from below the aircraft. (Tailplane wake not visualised for clarity.)



(b) View from below the port side of the aircraft.

Figure 12: Visualisation of the wake structure of the configuration, showing the close passage of the root vortex from the lower rotor over the empennage at advance ratio  $\mu = 0.30$ . (Propulsor wake not visualised for clarity.)

function of blade azimuth. The higher the inflow, the darker the shading of the plot. At all advance ratios, the aerodynamic environment of the lower rotor is strongly modified by interaction with the wake of the upper rotor, whereas the influence of the lower rotor on the upper is far less marked. A series of sharp ridges in the inflow distribution on the upper rotor is induced by the close passage of the tip vortices that trail from the blades of the same rotor; similar features can be seen in the inflow distribution on the lower rotor, but these are interleaved with additional ridges that are induced by the close passage of tip vortices that are generated by the blades of the upper rotor. Some disruption to the inflow distribution is also visible at the rear, particularly of the lower rotor, at all forward speeds. This is due to the root vortex system that is generated by the blades of the rotors; as shown in Fig. 6, the presence of the fuselage immediately below the main rotor system forces these vortices to remain very close to the plane of the lower rotor

for a considerable distance aft of the rotor shaft.

The effects of the passage of the individual blades of the top rotor over those of the lower rotor are clearly evident as a set of six radial ridges in the inflow experienced by the lower rotor; similar features are almost entirely absent from the inflow distribution on the upper rotor. At the lowest advance ratio a significant proportion of the lower rotor lies within the downwash field that is generated by the upper rotor, but as the forward speed of the system is increased, this region of maximum interaction between the rotors moves aftwards on the lower rotor in response to the rearwards skewing of the wake of the upper rotor.

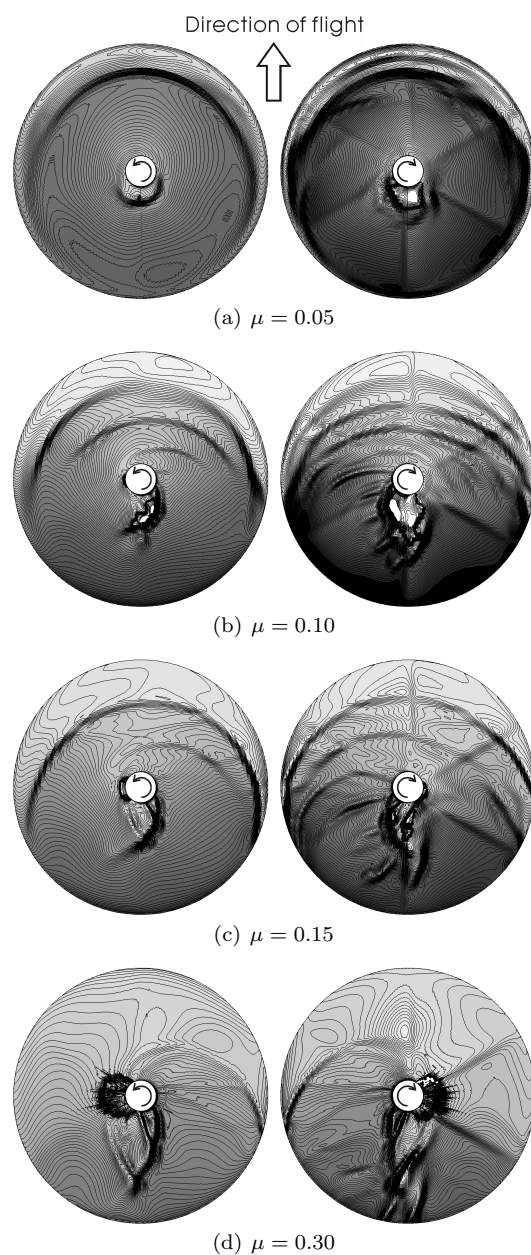
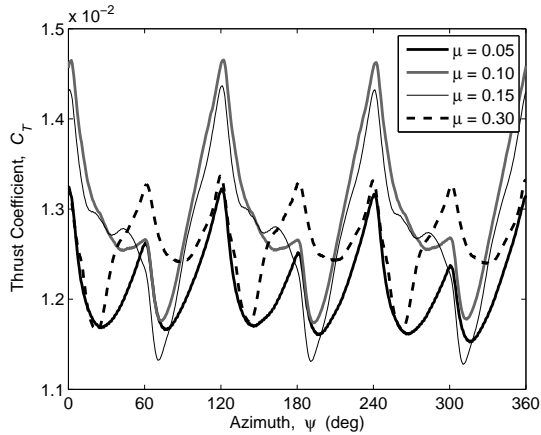
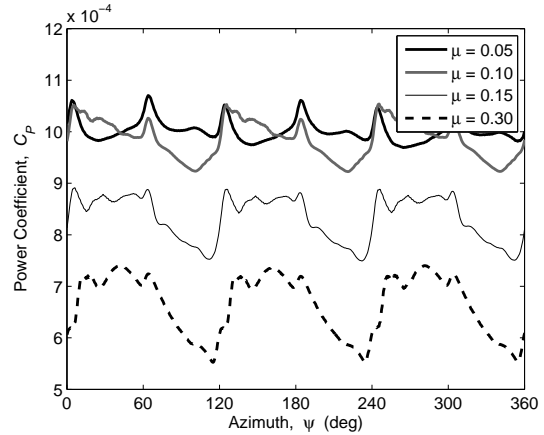


Figure 13: Inflow distribution over the main rotor discs, showing the strong interaction between the upper and lower rotors at all forward speeds. (Left: upper rotor. Right: lower rotor.)

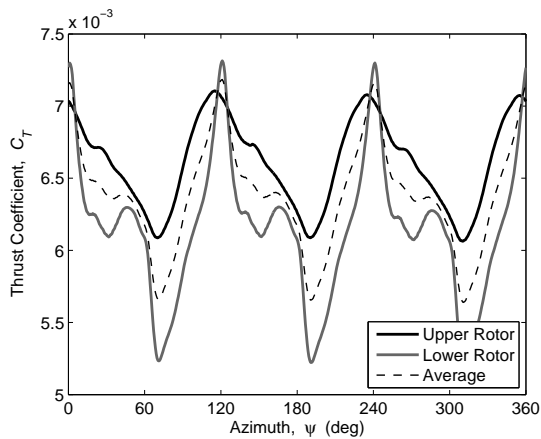


(a) Total thrust coefficient.

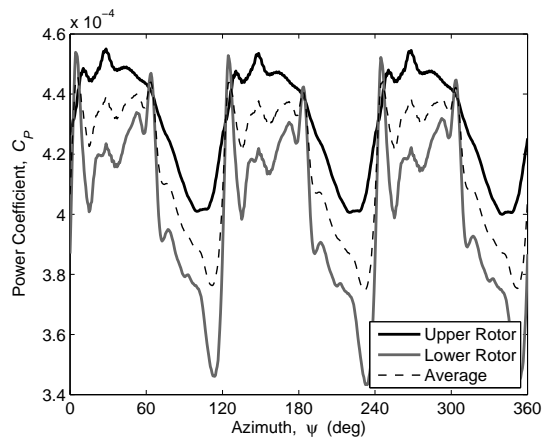


(b) Total power coefficient.

Figure 14: Temporal variation in the thrust produced and power consumed by the coaxial system over one revolution.



(a) Thrust coefficient.



(b) Power coefficient.

Figure 15: Temporal variation in the thrust produced and power consumed by the upper and lower rotors of the coaxial system over one revolution at advance ratio  $\mu = 0.15$ .

Figures 14 and 15 show the effect of the interactions between the two rotors on the loading produced on the main rotor system. Figure 14 shows the variation of thrust and power produced by the coaxial rotor over a single rotor revolution at each of the various flight speeds that were tested.

At all forward speeds, both the thrust and torque produced by the main rotor show significant unsteadiness, principally at  $3\Omega_c$  but also with a significant  $6\Omega_c$  contribution. Although it is likely that the fuselage vibration modes in a practical system will be tuned away from these fundamental rotor frequencies, the amplitude of the excitation as predicted here, especially for advance ratios in the transitional range between  $\mu = 0.10$  and  $\mu = 0.15$ , may be sufficient to require specific provisions for attenuation within the drive train and rotor mounting system. To reveal the origins of the excitation, Fig. 15 shows the variation of thrust and power produced by the coaxial system, decomposed into the individual contributions from the upper and

lower rotors. The figure shows the situation at an advance ratio  $\mu = 0.15$  where arguably the interaction between the upper and lower rotors is at its strongest. The curves marked ‘average’ represent half the total thrust or torque produced by the system and are included to show how the contributions from the individual rotors combine to give the overall characteristic of the main rotor system.

To achieve yaw moment equilibrium on the aircraft at this advance ratio, the upper rotor is driven by the trim routine to generate more power in the mean than the lower rotor; this effect manifests also in a difference in the mean thrust produced by the two rotors. In the context of the vibrational content of the loading on the system, Figure 14 shows the lower rotor to be the primary source of the  $6\Omega_c$  excitation of the system. The phasing of the  $6\Omega_c$  load on the rotor and the observation that this component of the load persists so strongly to higher advance ratios — where direct aerodynamic interaction between the rotors is significantly ame-

liorated by the rearwards sweep of their wakes — is consistent with its origin being in the overpassage-type interference with the blades of the upper rotor that appeared in Fig. 13 as the set of radial ridges in the inflow distribution on the lower rotor. The  $3\Omega_c$  component of the forcing of both the thrust and the torque is almost equally shared between the upper and lower rotors, and arises in the fundamental aerodynamic behaviour of the very stiff rotors from which the coaxial main rotor system is constructed (Ref. 15). Figure 16 shows the radial variation of loading and power consumption on the blades of upper and lower rotor as a function of azimuth with the helicopter trimmed into forward flight at  $\mu = 0.15$ . The phasing of the  $3\Omega_c$  variation in the thrust and the torque produced by the main rotor system is entirely consistent with the localisation of the peaks of maximum loading produced by both rotors to the rear quadrant of their respective advancing sides. During the XH-59A development programme, significant success in reducing overall vibration of the system was achieved by using differential cyclic input to the upper and lower rotors to change the load distribution on the rotors, and hence the relative phasing of the  $3\Omega_c$  vibrational component of their thrust and torque, in order to avoid the constructive interference between the loading signals from the upper and lower rotors that is shown in this study (Refs. 2, 18, 19, 21).

## Rotor-Propulsor Interaction

Figure 17 shows the variation of the thrust produced by the propulsor, over a single revolution of the main rotor system, with the system trimmed into forward flight at the various advance ratios that were simulated. This figure reveals that the loading produced on the propulsor is also highly unsteady at all but the highest forward speeds. A strong  $3\Omega_c$  component to the loading as well as a component at the blade-passage frequency of the propulsor is clearly discernible at all the advance ratios that were simulated.

Figure 18 shows the distribution of load on the propulsor disc at each of the advance ratios that were simulated. Each individual plot shows the radial distribution of load that is experienced by a single blade of the propulsor, during a single rotor revolution, as a polar function of blade azimuth. The blade loading has been decomposed into a mean component and a superimposed RMS fluctuation to allow the origins of the unsteadiness in the loading on the system to be identified. Given its design, the propulsor would produce its best performance if it were to operate in similar fashion to a propeller in free air, in other words, if it were to be exposed to a steady, axially-symmetric onset flow. The loading that is produced on the propulsor sug-

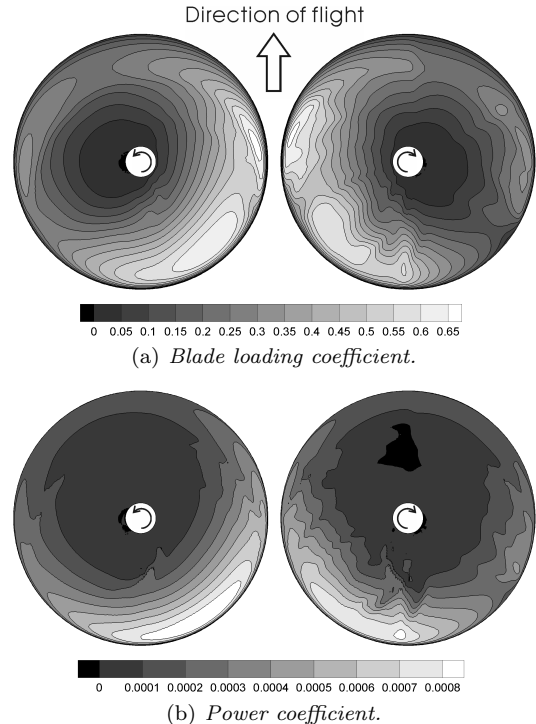


Figure 16: *Distribution of blade loading and power consumption over the upper and lower rotors of the coaxial system at advance ratio  $\mu = 0.15$ . (Left: upper rotor. Right: lower rotor.)*

gests that the onset flow experienced by this rotor is far from this ideal, however, except perhaps at the highest forward flight speed that was simulated. Indeed, Fig. 18 reveals the significant non-uniformity in the loading on the propulsor, at all forward flight speeds, that is induced by its aerodynamic interaction with the main rotor system and tailplane. The effects of the direct impingement of the wakes from the main rotor and the tailplane are clearly evident as localised patches of high RMS content to the loading. The location of these patches is entirely consistent with the dynamics of the wake that is revealed in Fig 6 and 7; as the wake of the main rotor skews increasingly rearwards with increasing advance ratio, the patches of most significant unsteadiness in the loading on the propulsor track upwards across its face. The azimuthal inhomogeneity in the loading experienced by the blades as they rotate is primarily responsible for the fluctuations in the thrust produced by the propulsor at and above its blade-passage frequency. The  $3\Omega_c$  component of the thrust produced by the propulsor is below the rotational frequency of the device and hence cannot originate from this source, however. In fact, this component of the loading must result directly from the temporal unsteadiness in the inflow through the propulsor that is caused by the periodic ingestion of the tip vortices from the main rotor.

It may well be asked why the dominant frequency of excitation of the load produced by the propul-

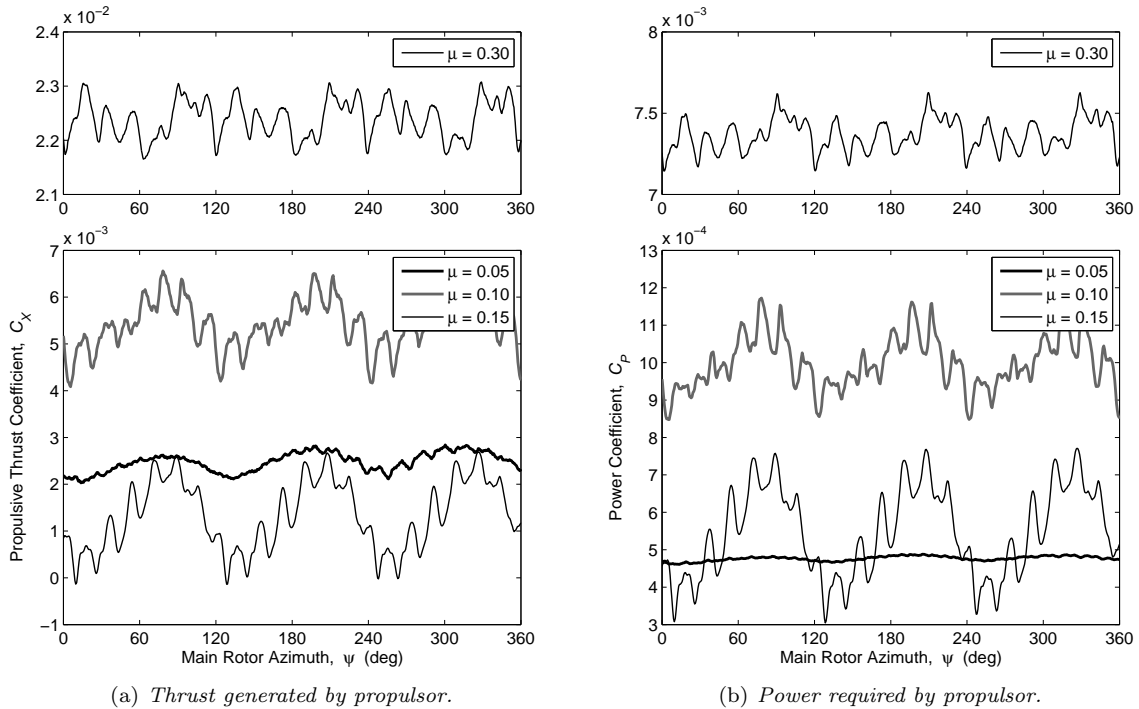


Figure 17: Temporal variation in propulsor thrust and power over one main rotor revolution.

tor is  $3\Omega_c$  rather than  $6\Omega_c$ , given that the coaxial main rotor contains six blades in total. This anomaly appears to be a consequence of the phasing of the rotation of the upper and lower rotors of the coaxial system. It is suggested above that the root cause of the low-frequency unsteadiness in the propulsor load is the entrainment of the tip vortices that the blades of the upper and lower rotors produce from the rear of their respective discs. In the configuration that was simulated, the blades of the upper and lower rotors pass directly over each other at the rear of the fuselage, with the result that the tip vortices from the two systems are laid down almost simultaneously into the flow at the rear of rotor. Except at the lowest forward speeds, where the downwards trajectory of the wake and the separation between the rotor discs causes the tip vortices to remain as relatively distinct structures, the vortices from the upper and lower rotors interact behind the rotor to behave effectively as a single coherent structure by the time that they interact with the propulsor. This process can be seen by careful examination of Fig. 10 and has the consequence that the inflow through the propulsor, and hence the loading, fluctuates at the lower than expected frequency. The effect of changing the phasing of the main rotors on the frequency content of the unsteady component of the load produced by the propulsor has yet to be investigated, however.

Most interestingly, Fig. 17 illustrates well the difficulties that might be encountered with the pusher-propulsor configuration in properly scheduling the division of loading between the main rotor

system and the propulsor. Figure 3 shows that, at an advance ratio  $\mu = 0.15$ , the propulsor is required to produce very little thrust — the scheduling of the rotor tilt has resulted in most of the propulsive requirement being transferred to the main rotor. Fig. 17 shows the resultant  $3\Omega_c$  fluctuation in the propulsor loading to be almost as large as the required mean thrust from the propulsor. The propulsor thus acts as a powerful source of dynamic excitation of the helicopter without much beneficial effect on the performance of the vehicle. This case is extreme, but given that the main rotor wake ceases to impinge on the propulsor only at relatively high advance ratio, there is the possibility that similar dynamic excitation might be a feature of the configuration over a relatively broad range of forward speeds — at least, given the data presented in Fig. 17, over the transitional range of advance ratios from  $\mu = 0.10$  to  $0.15$ . Certainly a tail-mounted propulsor that is left to rotate at or near its operating speed without producing any useful thrust does not appear to yield an ideal design solution, and the device may well do simply to be stopped and its blades feathered until high enough forward flight speed is attained for it to be clear of the main rotor wake.

## Rotor-Tailplane Interaction

The close passage of the main rotor tip vortices over the empennage also induces significant unsteadiness in the pressure distribution on the horizontal tailplane. Figure 19 compares the pressure coeffi-

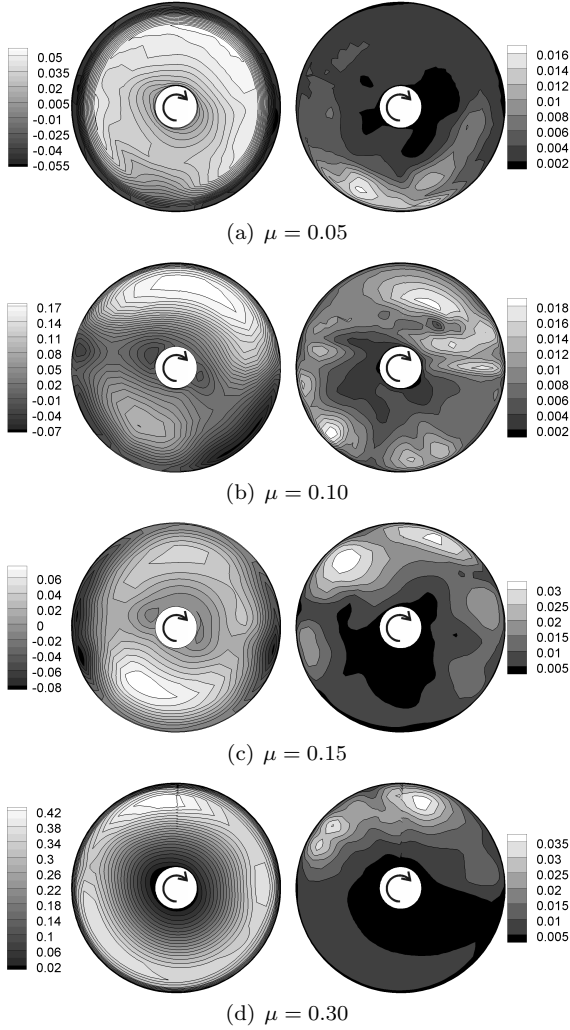


Figure 18: *Distribution of the blade loading coefficient over the propulsor disc, as seen from behind the helicopter. (Left: mean loading. Right: RMS fluctuation in loading.) Note that different scales are used in each plot.*

cient  $C'_P = 100(p - p_\infty) / (\frac{1}{2}\rho(\Omega R)^2)$  at the centre of area of the upper surfaces of the port and starboard sides of the tailplane, at advance ratio  $\mu = 0.10$ , by plotting its variation over a single main rotor revolution. The amplitude of the pressure fluctuations on the port and starboard sides of the tailplane are similar in magnitude but the  $3\Omega_c$  pressure peaks on the port and starboard sides are offset in phase by approximately  $30^\circ$  of a main rotor revolution. At this advance ratio, the tip vortex from the upper rotor passes closest to the port side of the tailplane, and the tip vortex from the lower rotor passes closest to the starboard side of the tailplane as shown in Fig. 10. The observed phase offset is a result of the slightly different times of arrival at the tailplane of the vortices from the upper and lower rotors at this low forward speed.

At  $\mu = 0.15$ , the effect of the root vortices from the main rotors in skewing the flow near the empennage can be seen quite strongly in the loading

distribution on the tailplane. Figure 20 again compares the pressure coefficient at the centre of area of the upper surfaces of the port and starboard sides of the tailplane by plotting its variation over a single main rotor revolution. As at the lower advance ratio, the pressure on both the port and starboard sides of the tailplane is characterised by a marked fluctuation at the blade-passage frequency of the main rotor. The shape of the pressure signal at this location is reminiscent of those generated by the ‘type 2’ close wake-surface interactions that are described by Leishman (Ref. 23). The pressure signals that result from this type of interaction are very sensitive to the location of the vortices relative to the surface, and, indeed, the asymmetry in the amplitude of the pressure fluctuations on either side of the tailplane is suggestive of a greater miss-distance between the tailplane and the interfering wake vortices on the starboard side of the tailplane than on the port.

At higher advance ratio, the pressure signal measured on the tailplane changes significantly in character. Fig. 21 shows the pressure on the tailplane at  $\mu = 0.30$ , as at lower forward speed, to be modulated at  $3\Omega_c$  by the close passage of the tip vortices from the main rotor. At  $\mu = 0.30$ , though, the propulsor is required to generate considerably more thrust than at lower advance ratios. The interaction between the highly-loaded propulsor and nearby components of the vehicle manifests in the pressure measured on the tailplane as a high-frequency fluctuation at the propulsor’s blade-passage frequency. On some fixed-wing aircraft with pusher propellers the fatigue life of any aerodynamic surfaces that are exposed to such an interaction can be reduced significantly, but it is also known that the actual magnitude of the interaction is very sensitive to the relative position of the propeller and the affected aerodynamic surface and thus is amenable to reduction through careful design.

These localised pressure fluctuations integrate to produce a periodic forcing of about five percent of the time-averaged loading on the tailplane at all of the forward speeds that were simulated. The principally  $3\Omega_c$  character of the unsteady forcing of the tailplane may contribute to the vibration of the empennage of the vehicle. In strong contrast, Fig. 5 shows the integrated effect of the pressures to result in very large changes with forward speed in the steady nose-up moment that is produced by the tailplane. This is particularly so as the aircraft passes through the range of advance ratios between 0.05 to 0.15, where Fig. 7 shows the wake of the main rotor to impinge directly on the tailplane. This particular pathology, known as ‘pitch up’ when coupled to the longitudinal dynamics of the aircraft, has been a feature of many heli-

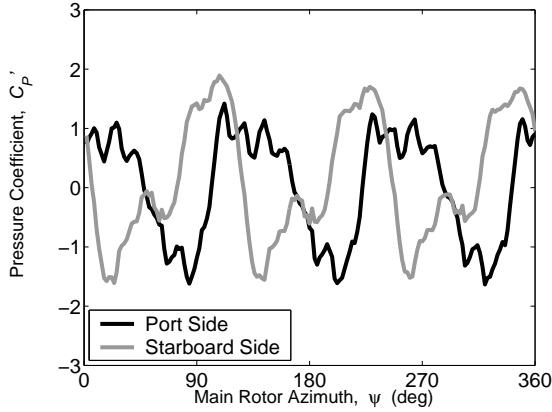


Figure 19: *Time-dependent pressure signals on the upper surface of the tailplane at advance ratio  $\mu = 0.10$ . (Mean removed.)*

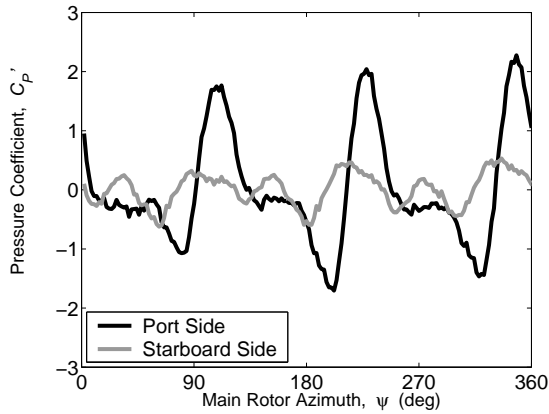


Figure 20: *Time-dependent pressure signals on the upper surface of the tailplane at advance ratio  $\mu = 0.15$ . (Mean removed.)*

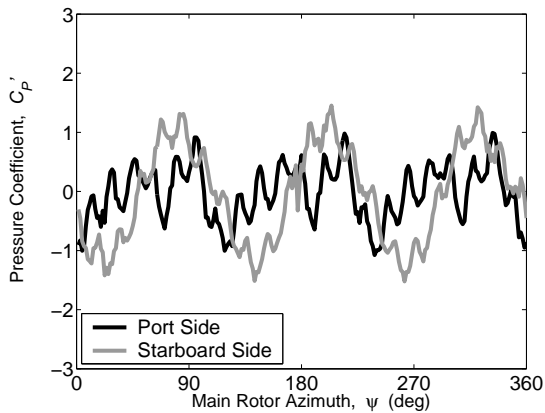


Figure 21: *Time-dependent pressure signals on the upper surface of the tailplane at advance ratio  $\mu = 0.30$ . (Mean removed.)*

copters during their development stage (Refs. 5–7, 9). Unless control margins are particularly narrow (for instance to prohibit overstressing of the blade system) the control power of the stiffened coaxial rotor is likely to be sufficient to allow the pilot to fly the aircraft through the affected speed range, but pilots often have poor regard for the strong non-linearity that this effect induces in the variation of stick position with forward speed. As many historical examples have shown, it can be very difficult to find a position for the tailplane which allows it to enhance the dynamic characteristics of the helicopter in high speed flight while avoiding the dynamic side-effects that are induced by interaction with the wake of the main rotor at low forward speed.

## Acoustic Signature

This final section of the paper considers the noise produced by the thrust-compounded hingeless coaxial configuration. The radiated acoustic field of the vehicle is computed using the Farassat-1A formulation (Ref. 24) of the Ffowcs Williams-Hawking equations. In the present numerical implementation, the aerodynamic force contributed by each blade panel was used to construct a point acoustic source at the centre of each panel. The sound that is radiated by each of these sources is then integrated to represent the loading noise that is produced by the blades. The aerodynamic model assumes an infinitesimally thin blade; the thickness noise has thus to be modelled independently. This is done by attaching a source-sink pair to each blade panel. Noise due to quadrupole terms is neglected in the present work as are any acoustic effects that are due to the presence of the fuselage. In the interests of brevity, discussion of the acoustics of the configuration is limited to one flight condition ( $\mu = 0.15$ ), and data for only one observer plane is presented. The sound pressure levels are scaled to represent the noise that is generated by an aircraft with a main rotor diameter of 5.5m and an all-up weight of 5562kg and thus to be representative of a helicopter of the size and weight of the XH-59A.

Figure 22(a) shows a contour map of the total sound pressure level (SPL) that is produced by the aircraft on a plane located one rotor radius below the hub of the lower main rotor of the system. Examination of the figure shows the thrust-compounded coaxial configuration to generate an acoustic signature that is qualitatively quite different to that produced by a conventional helicopter. With a conventional helicopter, the sound radiation pattern usually possesses a quite distinctive lateral asymmetry. This does not appear to be the case with the stiffened coaxial system, where the highly loaded advancing sides of both the upper

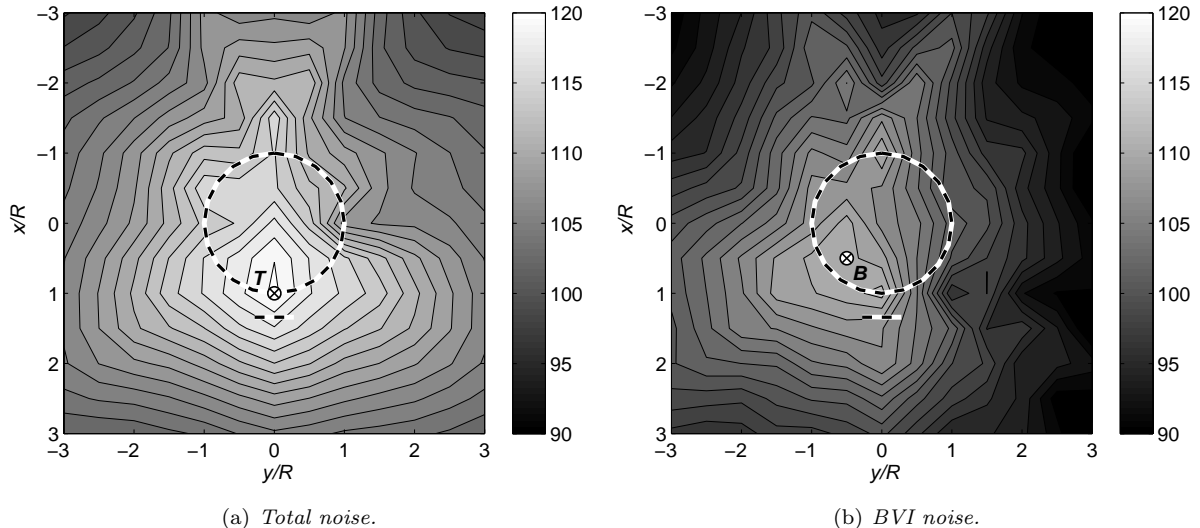
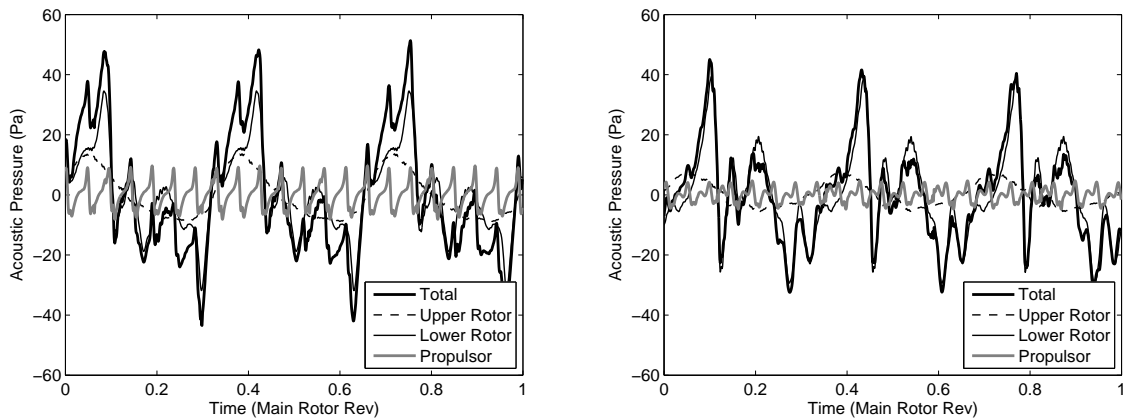


Figure 22: Sound pressure level (in decibels) produced at advance ratio  $\mu = 0.15$  on a plane parallel to the ground, one rotor radius below the hub of the lower main rotor.



(a) At point  $T$  (maximum SPL) in Fig. 22(a).

(b) At point  $B$  (maximum BVI SPL) in Fig. 22(b).

Figure 23: Time-history of acoustic pressure at the locations of maximum SPL shown in Fig. 22.

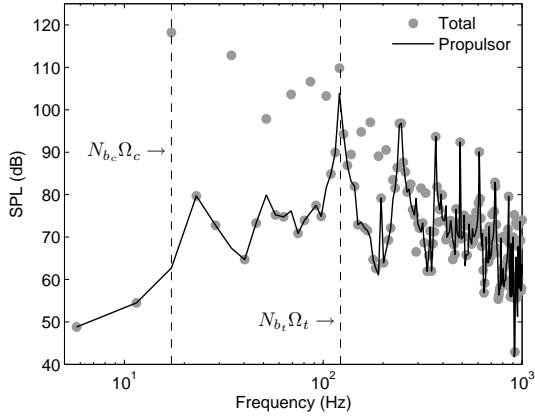
and lower rotors dominate the acoustic signature and combine to produce a much more symmetric radiation pattern.

The point of maximum SPL (or ‘hotspot’) on the plane below the rotor is represented by a symbol  $\otimes$ , labelled ‘ $T$ ’ in the figure, and is located directly below the tip of the main rotor at azimuth  $\psi = 0$ . The time history of the acoustic pressure at this point is shown in Fig. 23(a) and its associated frequency spectrum in Fig. 24. Figure 24(b) shows the noise that is radiated from lower main rotor to be significantly greater than that from the upper rotor of the coaxial system over the entire frequency range. While the major contribution to the noise from the coaxial system is at its blade-passage frequency, the lower rotor also radiates significant noise at twice its blade-passage frequency and also in the BVI frequency range. The noise contribution from the propulsor, particularly at its own blade-passage frequency, is also significant as can be seen from Figs. 23(a) and 24(a). In comparison to the

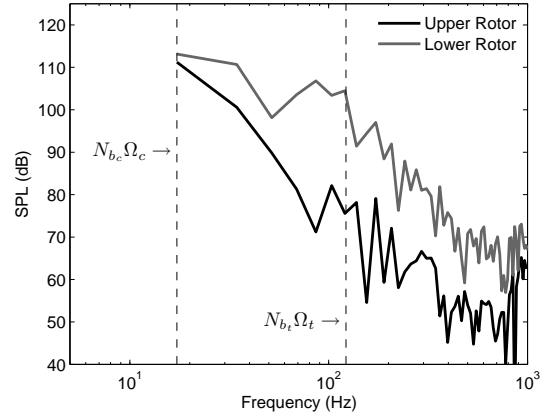
main rotor, though, the acoustic contribution from the propulsor is spread over a much broader bandwidth. Part of the impulsive noise created by this rotor at high frequencies is undoubtedly due to the direct passage of the wake from the main rotor and tailplane through the propulsor disc at this advance ratio.

Figure 22(b) shows a contour map of the SPL that is produced in the BVI frequency range (5-40 times the blade-passage frequency) by the aircraft. For a conventional rotor, one would typically expect to see two hotspots in the BVI-related acoustic signature — one each associated with the acoustic radiation from the blades on the advancing and retreating sides of the rotor (Ref. 25). This is not the case with the stiffened coaxial system — Fig. 22(b) shows the BVI-related component of the SPL on the ground plane to be concentrated on the port side of the aircraft.

The reason for this asymmetry is revealed in the inflow maps shown in Fig. 13. These show a much



(a) Total SPL and contribution from the propulsor.



(b) Contributions from the upper and lower rotor.

Figure 24: Acoustic noise spectrum at point  $T$  (location of maximum total SPL in Fig. 22(a)).

stronger pattern of BVI-induced ridges in the inflow on the lower than on the upper rotor of the coaxial system, particularly at this advance ratio where the tip vortices of the upper rotor pass directly through the disc of the lower rotor and produce a strong additional contribution to its BVI-induced loading. Indeed, the time history of the pressure signal at the point of maximum BVI noise, presented in Fig. 23(b), shows clear evidence of BVI-type impulses that originate almost entirely from the lower rotor. As shown in Fig. 16, the rear quadrant of the advancing side of the lower rotor is highly loaded compared to its retreating side, with the result that the acoustic emission from this part of the rotor is enhanced compared to the retreating side. The combination of high loading and enhanced BVI activity results in the rear of the advancing (port) side of the lower rotor dominating the BVI-related acoustic emission from the coaxial rotor system, and thus the bias of this component of the SPL on the ground plane to the port side of the aircraft as shown in Fig. 22(b).

Thus it appears that the acoustic signature from the system is exacerbated by a loading distribution that is produced largely in response to the requirement for the main rotor to counter the strong nose-up pitching moment from the tailplane at this flight condition (see Fig. 5). This is a particularly interesting example of how long-range aerodynamic coupling between disparate parts of the configuration can have largely unforeseen consequences on superficially unrelated characteristics of the aircraft

Finally, Fig. 25 shows a contour map of the contribution of the propulsor on its own to the SPL on the plane located one rotor radius below the lower rotor of the system. The orientation of the propulsor results in a rather undesirable focusing of the noise from the helicopter. This is because the in-plane component of the noise produced by the propulsor radiates directly to the ground. The

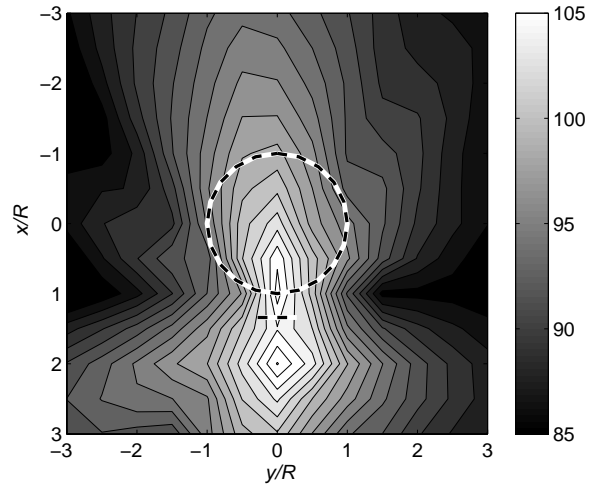


Figure 25: Sound pressure level (in decibels) produced by the propulsor at advance ratio  $\mu = 0.15$  on a plane parallel to the ground, one rotor radius below the hub of the lower main rotor.

figure shows the directivity of the acoustic signature on the plane below the aircraft to be directly in line with the axis of the propulsor, and the noise produced by this rotor to be concentrated in two hotspots, one located upstream and the other downstream of the propulsor disc. The noise contributed by this rotor at the downstream hotspot, predicted to be 108dB, is much more intense than at the upstream hotspot. Interestingly, the upstream hotspot is located exactly at the position of maximum overall noise produced by the configuration, with the consequence that the placement of the propulsor with respect to the main rotor could have a significant effect on acoustic focusing within the system and thus possibly on the maximum overall SPL produced by the configuration. The sensitivity of the acoustic signature of the configuration to the position of the propulsor has yet to be investigated in any detail, however.

By comparison, the sound pressure level at the location of maximum noise produced by the helicopter is predicted to be approximately 120dB, while at the location of maximum BVI noise, the SPL is predicted to be approximately 112dB. Although it has been shown, as with the rotor vibration, that altering the relative phasing of the rotation of the main rotors and the introduction of differential cyclic pitch can have some effect in reducing the noise that is produced by stiffened coaxial rotor systems, both these values are much higher than would be expected for an equivalent conventional helicopter (Ref. 26).

## Conclusions

The aerodynamic and acoustic characteristics of a generic, thrust-compounded coaxial helicopter have been simulated using Brown's Vorticity Transport Model. The configuration that has been studied comprises a stiff coaxial main rotor system consisting of two, counter-rotating, three-bladed rotors, an auxiliary propulsor mounted in pusher configuration at the rear of the fuselage, and a streamlined fuselage with a horizontal tailplane mounted just forward of the propulsor. The various aerodynamic interactions that are predicted to arise within the system over a range of forward speeds have been analysed in detail, the aim of the work being to show that modern computational techniques are advancing to a state where they can be used at an early stage in the design process to provide useful insight into the likely aeromechanical behaviour of realistic helicopter configurations.

The aerodynamic environment of the configuration that was studied is characterised by very strong aerodynamic interactions between its various components.

The aerodynamic environment of the main rotors of the system is dominated by the direct impingement of the wake from the upper rotor onto the blades of the lower rotor, and the thrust and torque produced by the system are highly unsteady — particularly at low forward speed. The fluctuations in the loading on the coaxial system occur at the fundamental blade-passage frequency and are particularly strong as a result of the phase relationship between the signals from the upper and lower rotors, and also at twice the blade-passage frequency as a result of the loading fluctuations that are induced on the system as a result of direct blade overpassage. The results presented here support the rationale behind previous studies that have suggested that the vibration that is produced by stiffened coaxial systems can be ameliorated by applying differential cyclic inputs to the upper and lower rotors or by modifying the phasing of the rotation of the upper rotor with respect to the lower.

The wake of the main rotor sweeps over the fuselage and tailplane at low forward speed, inducing a significant nose-up pitching moment on the tailplane that must be counteracted by longitudinal cyclic input to the main rotor. This pitch-up characteristic has been encountered during the development of several helicopters and has proved on occasion to be very troublesome to eradicate. Over a broad range of forward flight speeds, the wake from the main rotor is ingested directly into the propulsor, where it induces strong fluctuations in the loading produced by this rotor. These fluctuations occur at both the blade-passage frequency of the main rotor and of the propulsor, and are likely to excite significant vibration of the aircraft. The results presented here suggest that this interaction, together with poor scheduling of the partition of the propulsive thrust between the main rotor and a rear-mounted propulsor with forward speed can lead to a distinctly non-optimal situation where the propulsor produces significant vibratory excitation of the system but little useful contribution to its propulsion.

With the present configuration, the propulsor induces significant vibratory forcing on the tailplane at high forward speed. This forcing is at the fundamental blade-passage frequency of the propulsor, and suggests that the tailplane position in any vehicle where the lifting surface and propulsor are as closely coupled as in the present configuration may have to be considered carefully to avoid shortening the fatigue life of the tailplane. Nevertheless, the unsteady forcing of the tailplane is dominated by interactions with the wake from the main rotor — the  $3\Omega_c$  fluctuations that are observed in the pressure distribution on the tailplane are characteristic of the close passage of individual vortices over its surface.

Finally, the character of the acoustic signature generated by the system has been investigated. Data on a single plane below the system at one particular flight condition has been presented to suggest that the overall noise produced by the system, at least in slow forward flight, is significantly higher than that produced by similar conventional helicopters in the same weight class. The major contribution to the BVI noise comes from the lower rotor because of strong aerodynamic interaction with the upper rotor. The propulsor contributes significant noise (up to 108dB) over a broad frequency spectrum. At the flight condition that was considered, much of this noise is induced by interactions between the blades of the propulsor and the wake of the main rotor and tailplane.

The numerical calculations are thus able to reveal many of the aerodynamic interactions that might be expected to arise in a configuration as aerodynamically complex as the generic thrust-

augmented coaxial helicopter that formed the basis of this study. Of course the exact form, and particularly the effect on the loading produced on the system, of these interactions may vary depending on the specifics of the configuration. Indeed, more careful or considered design may be capable of eliminating entirely some of the effects that are highlighted in this study.

Nevertheless, the results presented here lend weight to the assertion that the state of the art of computational helicopter aerodynamic predictions is advancing to a stage where, despite the historical record in this regard, the use of such models may allow sufficiently trustworthy insight into the behaviour of such systems to be obtained early enough in the design process for any aeromechanical problems to be circumvented before they manifest on the prototype or production item.

## Acknowledgements

The authors would like to thank Mr. Carlos Sousa (Universidade Técnica de Lisboa and a Visiting Student at Glasgow University) for his assistance in creating the fuselage geometry used in this study.

## References

- <sup>1</sup>Coleman, C.P., “A Survey of Theoretical and Experimental Coaxial Rotor Aerodynamic Research,” NASA TP-3675, March 1997.
- <sup>2</sup>Burgess, R.K., “The ABC<sup>TM</sup> Rotor — A Historical Perspective,” *American Helicopter Society 60<sup>th</sup> Annual Forum*, Baltimore, MD, 7–10 June 1971.
- <sup>3</sup>Orchard, M., Newman, S., “The fundamental configuration and design of the compound helicopter,” *Proceedings of Institution of Mechanical Engineers Vol. 217 Part G: Journal of Aerospace Engineering*, G01702, October 2003, pp. 297–315.
- <sup>4</sup>Sheridan, P.F., Smith, R.P., “Interactional Aerodynamics — A New Challenge to Helicopter Technology,” *Journal of the American Helicopter Society*, January 1980, pp. 3–21.
- <sup>5</sup>Cooper, D.E., “YUH-60A Stability and Control,” *Journal of the American Helicopter Society*, Vol. 23, No. 3, 1978, pp. 2–9.
- <sup>6</sup>Prouty, R.W., Amer, K.B., “The YAH-64 Empennage and Tail Rotor — A Technical History,” *American Helicopter Society 38<sup>th</sup> Annual Forum*, Anaheim, California, USA, 1982, pp. 247–261.
- <sup>7</sup>Main, B.J., and Mussi, F., “EH101 — Development Status Report,” *Proceedings of the 16<sup>th</sup> European Rotorcraft Forum*, Glasgow, UK, 1990, pp. III.2.1.1–12.
- <sup>8</sup>Cassier, A., Weneckers, R., and Pouradier, J., “Aerodynamic Development of the Tiger Helicopter,” *Proceedings of the American Helicopter Society 50<sup>th</sup> Annual Forum*, Washington DC, 1994.
- <sup>9</sup>Eglin, P., “Aerodynamic Design of the NH90 Helicopter Stabilizer,” *Proceedings of the 23<sup>rd</sup> European Rotorcraft Forum*, Dresden, Germany, 1997, pp. 68.1–10.
- <sup>10</sup>Frederickson, K.C., and Lamb, J.R., “Experimental Investigation of Main Rotor Wake Induced Empennage Vibratory Airloads for the RAH-66 Comanche Helicopter,” *Proceedings of the American Helicopter Society 49<sup>th</sup> Annual Forum*, St. Louis, Missouri, USA, 1993, pp. 1029–1039.
- <sup>11</sup>Brown, R.E., “Rotor Wake Modeling for Flight Dynamic Simulation of Helicopters,” *AIAA Journal*, Vol. 38, No. 1, January 2000, pp. 57–63.
- <sup>12</sup>Brown, R.E., Line, A.J., “Efficient High-Resolution Wake Modeling Using the Vorticity Transport Equation,” *AIAA Journal*, Vol. 43, No. 7, April 2005, pp. 1434–1443.
- <sup>13</sup>Kenyon, A.R., Brown, R.E., “Wake Dynamics and Rotor-Fuselage Aerodynamic Interactions,” *American Helicopter Society 63<sup>rd</sup> Annual Forum*, Virginia Beach, VA, May 2007.
- <sup>14</sup>Kim, H.W., Brown, R.E., “Coaxial Rotor Performance and Wake Dynamics in Steady and Manoeuvring Flight,” *American Helicopter Society 62<sup>nd</sup> Annual Forum*, Phoenix, AZ, May 2006.
- <sup>15</sup>Kim, H.W., Brown, R.E., “Impact of Trim Strategy and Rotor Stiffness on Coaxial Rotor Performance,” *1<sup>st</sup> AHS/KSASS International Forum on Rotorcraft Multidisciplinary Technology*, Seoul, Korea, 15–17 October 2007.
- <sup>16</sup>Ruddell, A.J., “Advancing Blade Concept (ABC<sup>TM</sup>) Development,” *American Helicopter Society 32<sup>nd</sup> Annual Forum*, Washington, D.C., May 1976.
- <sup>17</sup>Burgess, R.K., “Development of the ABC Rotor,” *American Helicopter Society 27<sup>th</sup> Annual Forum*, Washington, D.C., May 1971.
- <sup>18</sup>Halley, D.H., “ABC Helicopter Stability, Control, and Vibration Evaluation on the Princeton Dynamic Model Track,” *American Helicopter Society 29<sup>th</sup> Annual Forum*, Washington, D.C., May 1973.
- <sup>19</sup>Paglino, V.M., “Forward Flight Performance of a Coaxial Rigid Rotor,” *American Helicopter Society 27<sup>th</sup> Annual Forum*, Washington, D.C., May 1971.

<sup>20</sup>Dingeldein, R.C., “Wind-Tunnel Studies of the Performance of Multirotor Configurations,” NACA TN-3236, August 1954.

<sup>21</sup>Paglino, V.M., Beno, E.A., “Full-Scale Wind-Tunnel Investigation of the Advancing Blade Concept Rotor System,” USAAMRDL TR 71-25, August 1971

<sup>22</sup>Fletcher, T.M., Brown, R.E., “Main Rotor — Tail Rotor Wake Interaction and its Implications for Helicopter Directional Control,” *32<sup>nd</sup> European Rotorcraft Forum*, Maastricht, Netherlands, September 2006.

<sup>23</sup>Bi, N.P., Leishman, J.G., “Analysis of Unsteady Pressures Induced on a Body by a Rotor,” *Journal of Aircraft*, Vol. 28, No. 11, 1991, pp. 756–767.

<sup>24</sup>Farassat, F., Succi, G.P. “A Review of Propeller Discrete Frequency Noise Prediction Technology with Emphasis on Two Current Methods for Time Domain Calculations,” *Journal of Sound and Vibration*, Vol. 71, No. 3, 1980, pp. 399–419.

<sup>25</sup>Kelly, M.E., Duraisamy, K., Brown, R.E., “Blade Vortex Interaction and Airload Prediction using the Vorticity Transport Model,” *American Helicopter Society Specialists’ Conference on Aeromechanics*, San Francisco, CA, 23–25 January 2008.

<sup>26</sup>Schmitz, F.H., “Aeroacoustics of Flight Vehicles: Theory and Practice,” NASA Reference Publication 1258, Vol. 1, Chapter 2, August 1991, pp. 65–149.